*Journal of Computer Science*

Research Article

# Polar Disentangled Non-Local Convolutional Neural Network for Skin Cancer Classification Using Dermoscopy Images

**Usha Thirugnanam[1] and Nalini Joseph[2]**

[1]*Department of Computer Science Engineering, Bharath Institute of Higher Education and Research, Chennai, Tamil Nadu, India*
[2]*Department of Computer Science Engineering, Bharath Institute of Science and Technology, Chennai, Tamil Nadu, India*

*Article history*
Received: 14-10-2025
Revised: 02-03-2026
Accepted: 04-05-2026

**Corresponding Author:**
Usha Thirugnanam
Department of Computer Science Engineering, Bharath Institute of Higher Education and Research, Chennai, Tamil Nadu, India
Email: tusha.cse@outlook.com

**Abstract:** Skin cancer classification is the process of identifying and categorizing various types of skin lesions into cancerous and non-cancerous. This process is performed to achieve accurate detection, which minimizes the risk of severe health complications. However, classifying the severity of skin lesion images is a difficult task because of subtle and overlapping visual patterns, which could lead to inaccurate performance. To address this issue, this research proposes a Polar Disentangled Non-Local Convolutional Neural Network (PDNLCNN) to classify the skin images accurately by using dermoscopy images. In a conventional CNN, PDNL is incorporated to enhance the network's ability to capture global contextual relationships effectively. This enables the model to capture fine-grained lesion information and structural patterns effectively, which are essential for accurate classification. Furthermore, the Fuzzy C-Means (FCM) clustering algorithm is employed to segment skin cancer, which manages uncertainty by assigning varying degrees of membership. This improves the boundary detection of the skin lesions and enables better accuracy in the segmentation process. Hence, the proposed PDNLCNN achieves superior classification accuracy of 99.21% on the HAM10000 dataset when compared with the existing methods, such as Deep CNN (DCNN).

**Keywords:** Digital Hair Removal, Dermoscopy Image, Polar Disentangled Non-Local Convolutional Neural Network, Resizing, Skin Cancer

## Introduction

Skin is the largest organ in the human body, acting as a main barrier against environmental factors and playing a primary role in protecting the body from diverse pathogens and UltraViolet (UV) radiation. As the outermost layer of the body, it is highly exposed and vulnerable to diverse diseases, including different types of skin cancer, which rank among the most common cancers worldwide (Musthafa et al., 2024). The World Health Organization (WHO) identifies skin cancer as a growing global concern which accounts for nearly 33.33% of all cancer cases. Over the last decade, its incidence has risen significantly in countries like Australia, the United States, and Canada. Every year, over 15,000 people die because of skin cancer (Mridha et al., 2023), which has two primary types: Non-melanoma (benign) and melanoma (Ozdemir and Pacal, 2025; Gajbhiye et al., 2025). Benign (noncancerous) tumors (Yang et al., 2023) typically grow slowly and do not spread to other parts of the body, whereas malignant (cancerous) tumors grow rapidly by attacking and destroying the adjacent normal tissues and also spread throughout the body (Faizi and Adnan, 2024). Malignant skin cancers arise from melanocytes that are responsible for melanin production. This type of cancer begins with the uncontrolled growth of melanocytes, which results in tumor formation. Malignant skin cancer can develop anywhere in the body, but most commonly occurs in the sun-exposed areas such as hands, face, lips, and neck (Attallah, 2024). Melanoma is classified into different types, such as superficial spreading, nodular, malignant lentigo, and acral lentiginous. Although most skin tumors are benign, the primary malignant forms contain Squamous Cell Carcinoma (SCC), Sebaceous Gland Carcinoma (SGC) (Saha et al., 2025), and Basal Cell Carcinoma (BCC) (khan et al., 2025a; Raghavendra et al., 2023).

Skin cancer diagnosis involves various techniques

such as dermoscopy, visual examination, and biopsy. Common diagnostic processes for skin cancer include the Asymmetry, Border, Color, Diameter (ABCD) rule and seven-point checklist, which rely heavily on the expert interpretation during visual examination (Toprak and Aruk, 2024). In the ABCD diagnostic procedure, a sample is subjected to pathological evaluation to obtain a definitive diagnostic result, which is an invasive technique that is utilized for categorizing all types of cancer. But it has certain limitations, such as high cost, pain, and time consumption (Himel et al., 2024). Physician expertise and dermoscopy significantly enhance the identification accuracy (Abdulredah et al., 2025). This process eliminates the samples from the suspected skin lesions to examine malignancy (Alotaibi and AlSaeed, 2025). Skin cancer is typically diagnosed through direct visual analysis via the naked eye and biopsy (Pandey et al., 2024; Jaber and Akbas, 2024). By using technological developments, dermatologists utilize dermoscopic (Abdulkadhim et al., 2025) microscopic images to identify skin cancer. Microscopic images are gathered utilizing mobile phone cameras and digital cameras, which causes a resolution problem with data types, whereas dermoscopic images are gathered using dermoscopy (Khan et al., 2025b). Researchers establish different Computer-Aided Diagnosis (CAD) systems using Artificial Intelligence (AI) for supporting dermatologists (Aboulmira et al., 2025). Such systems use Machine Learning (ML) and Deep Learning (DL) to classify skin lesions with high accuracy and enable efficient analysis (Eliwa et al., 2025). However, DL is preferred over conventional ML methods for segmenting and classifying skin cancers because it automatically learns intricate features without requiring manual feature extraction.

### *Problem Statement and Objective*

Skin cancer classification using dermoscopic images is challenging because of the subtle, overlapping, and intricate visual patterns of lesions that resemble one another, leading to suboptimal performance. Therefore, it is essential to design a reliable method for an accurate skin cancer classification. To address this, a Polar Disentangled Non-Local Convolutional Neural Network (PDNLCNN) is proposed for classifying skin cancer accurately, which models both the angular and radial dependencies of lesion structures. This enables the network to effectively separate overlapping and intricate visual patterns by emphasizing the symmetry and circular characteristics present in dermoscopic images, thereby enhancing the model's performance.

### *Contributions*

The primary contributions are explained as follows:

- PDNLCNN introduces novel integration of CNN with PDNL, which captures long-range dependencies in skin lesion images. By utilizing the Cartesian to polar coordinate transformation, it effectively captures invariant textural and structural features. This novel design distinguishes NL and DNL which improves lesion representation and classification accuracy
- To segment the image, Fuzzy C-Means (FCM) is applied to manage the fuzzy and lesion boundaries by assigning a partial membership to pixels, which ensures smoother segmentation. This provides an accurate separation of lesion regions from the healthy skin and improves reliability
- Resizing is employed to ensure uniform image dimensions that minimize the computational complexity, whereas the digital hair removal eliminates unwanted artifacts such as hair, which assists the model in concentrating on lesion characteristics. This process increases the image clarity and leads to more reliable and accurate performance

### *Literature Survey*

Kumar et al. (2024b) established a transformer-based method integrated with handcrafted texture features and Gray Wolf Optimization (GWO) to categorize skin cancer accurately. In the preprocessing stage, normalization was used to standardize the image dimensions, and a median filter was applied to eliminate noise, which enhanced image quality. Consequently, a Gray-Level Co-occurrence Matrix (GLCM) and Local Binary Pattern (LBP) were utilized to extract the features that captured spatial patterns, whereas GWO was applied to select the most discriminative features. A transformer-based decoder was used to classify skin cancer by leveraging an attention mechanism that assisted in capturing contextual dependencies. However, the transformer method with handcrafted texture features failed to capture deep hierarchical patterns in intricate lesion images.

Ibrahim et al. (2025) developed an ensemble transfer-learning model by using methods such as EfficientNetV2B2, MobileNet, ResNeXt101, Xception, and DenseNet201 to categorize skin lesions. During training and testing, Test Time Augmentation (TTA) and annealing learning rates were employed to enhance the model's performance. From a dense layer, features were retrieved by utilizing transfer learning, and weighted majority voting was used in the ensemble method for aggregating predictions by using Softmax to classify skin cancer. Nevertheless, the ensemble method suffered from high computational cost and memory usage because of multiple deep networks.

Houssein et al. (2024) suggested a Deep CNN (DCNN) to classify skin cancer lesions. Normalization

was applied to ensure uniformity in pixel values, which avoided certain features and enhanced the model stability during the learning process. Additionally, all images obtained from the dataset were reshaped to a standardized size, which not only maintained the consistency in image dimension but also reduced the memory consumption and enhanced the computational effectiveness. However, the DCNN struggled with overfitting when trained on limited skin cancer images due to the requirement of large amounts of labeled data for effective generalization.

Al Mahmud et al. (2024) presented SkinNet-14 for classifying skin cancer. SkinNet-14 employed a modified Compact Convolutional Transformer (CCT) method for processing pixel images effectively, which minimized the training time and computational load. The proposed method utilized numerous image processing and augmentation processes to improve the quality of an input image and balance the dataset to solve class imbalance. Finally, SkinNet-14 was used to classify skin cancer. Nevertheless, SkinNet-14 was limited by its relatively shallow architecture, which minimized the model's ability to learn complex hierarchical features from the different skin lesions.

Kumar et al. (2024a) introduced a DL method that combined a U-Net and an improved MobileNet-V3 with optimization to classify skin cancer effectively. The squeeze and excitation blocks were replaced with the channel attention blocks to achieve parameter reduction. In MobileNet, a cross-layer connection was integrated to leverage synthetic features effectively. Additionally, the Bayesian optimization method was used to fine-tune the hyperparameters of the MobileNet-V3 model. However, the U-Net was limited by its reliance on the pixel-level annotations, which made it sensitive to the boundary irregularities in skin lesions.

Abohashish et al. (2025) presented a hybrid Long Short-Term Memory-CNN (LSTM-CNN) to classify skin cancer. The patching sequence enabled the modeling system to determine the local patterns in an image. Subsequently, CNN layers were utilized for extracting spatial functions, namely color variation, edges, and textures. The Softmax layer was employed for the classification, which offers a probability distribution across the possible classes. Nevertheless, integrating temporal modeling with a CNN introduced redundant representations that minimized the classification accuracy for fine-grained lesion patterns.

Overall, the existing techniques exhibited limitations such as manually engineered features, overfitting, introducing redundant representation, and subtle and overlapping visual patterns that led to inaccurate performance. To address these issues, a PDNLCNN was proposed for skin cancer classification by automatically learning deep hierarchical features without manual features. The PDNL block captured both radial and angular dependencies that minimized the redundant representation and created a model to effectively distinguish subtle and overlapping lesion patterns that enhanced the classification accuracy.

## Methods

This research proposes a PDNLCNN for an accurate classification of skin cancer using dermoscopy images. Initially, the HAM10000 dataset is employed to identify the model performance, while ISIC2019 is utilized to determine generalizability. In the preprocessing stage, resizing and digital hair removal techniques are used to standardize the input dimension and eliminate unwanted artifacts such as hair, which enhances clear visibility. Later, FCM is applied to segment the skin lesion, whereas the proposed PDNL block accurately extracts and classifies the skin cancer. Fig. 1 illustrates the overall workflow of the proposed method.

In this research, the HAM10000 (2025) dataset and the ISIC2019 (2025) dataset are employed to evaluate proposed method. ISIC2019 is used to evaluate the generalizability of skin cancer classification across different lesion types. Both datasets include dermatology and dermatoscopic imaging, which capture clinical diversity, diagnostic challenges, image variability, and ethical considerations. A detailed description of these datasets is provided below.

### *Dataset*

HAM10000: It has 10,015 skin images across seven lesion types, including 1,113 melanomas, 514 BCC, 327 AK, 6,705 melanocytic nevi, 115 dermatofibromas, 142 vascular lesions, and 1,099 benign keratoses. The images are captured at a resolution of 600 × 450 pixels. Fig. 2 demonstrates the sample images from HAM10000.

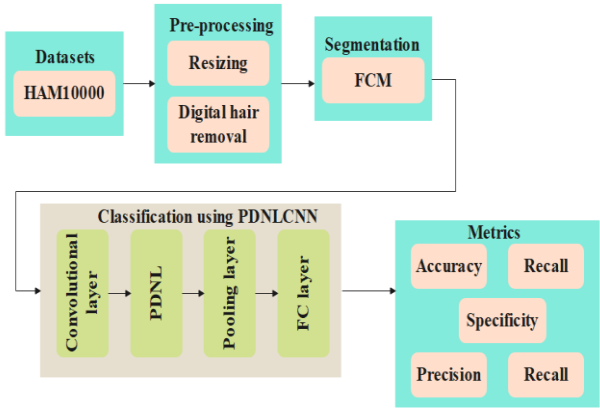


**Fig. 1:** Overall workflow of the proposed method for skin cancer classification

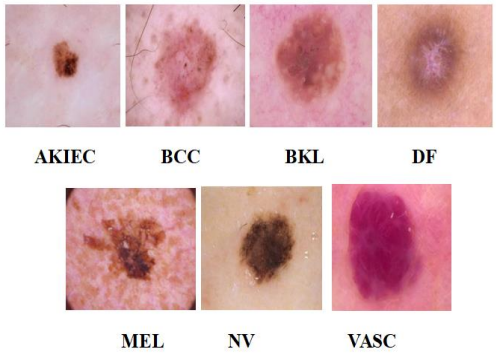


**Fig. 2:** Sample dermoscopic images from the HAM10000 dataset representing various skin lesion types

The ISIC2019 this dataset contains 25,331 images that are split into eight different classes to evaluate generalization ability. Each image in a dataset is related to a particular diagnostic class that represents the skin lesion type. ISIC2019 includes a wide range of skin conditions and offers a comprehensive platform for dermatoscopic image evaluation. The obtained images are split into 80% training and 20% testing images, and these images are preprocessed using resizing and hair removal.

### *Preprocessing*

After image acquisition, resizing and digital hair removal techniques are used to standardize the input dimensions and eliminate inappropriate artifacts, which ensures that the model concentrates on the actual lesion features. A detailed description of this process is provided below.

Resizing: As images of various sizes offer different numbers of features, resizing is necessary to ensure uniformity. Standardizing the input dimensions not only minimizes the processing time but also increases the overall system performance. In this research, all input images are resized to $256 \times 256$ pixels.

Digital hair removal: After resizing, digital hair removal is applied depending on morphological filtering like black-hat transformation. Also, in-painting methods are employed to eliminate hair from the skin images, which eliminates noise artifacts and minimizes sensitivity. The steps are as follows.

- Step 1: The Red Green Blue (RGB) images are converted into grayscale to simplify processing, which preserves the structural information
- Step 2: A morphological black hat transformation is applied to grayscale images to represent the dark hair artifacts against a lighter skin background
- Step 3: Subsequently, a mask is created from the detected hair to perform in-painting
- Step 4: Finally, the in-painting model is applied to the original RGB image by using this mask to fill the hair regions

This process eliminates hair artifacts effectively, ensuring that the model concentrates on actual lesion features and enhances the segmentation and classification process. Fig. 3 displays the sample images of digital hair removal, which are then fed into the segmentation process using the FCM.

### *Segmentation*

After preprocessing, FCM is used to segment the skin lesions because it handles fuzzy boundaries by assigning partial membership to pixels, which captures the gradual transition between lesions and healthy skin effectively. The lesion gradually fades into the surrounding healthy skin, creating low-contrast and fuzzy boundaries. Conventional hard clustering methods, such as k-means, assign all the pixels to exactly one cluster, which does not maintain the uncertainty at the lesion borders, which causes inaccurate segmentation. U-Net struggles to capture gradual transitions between healthy and lesion skin that lead to reduced segmentation performance. Hence, FCM is used over k-means and U-Net for skin lesion segmentation due to lesions having fuzzy boundaries and low contrast that blend into healthy skin. FCM (Alqhtani et al., 2024) assigns partial membership values to pixels that capture uncertainty at edges. This enables more accurate delineation of lesion regions where boundaries are ambiguous. Moreover, FCM captures the inherent uncertainty in the boundary regions, which offers smoother and more realistic segmentation outcomes. The main purpose of FCM is to identify the cluster centers that accurately indicate the distribution of pixel intensities in an image.

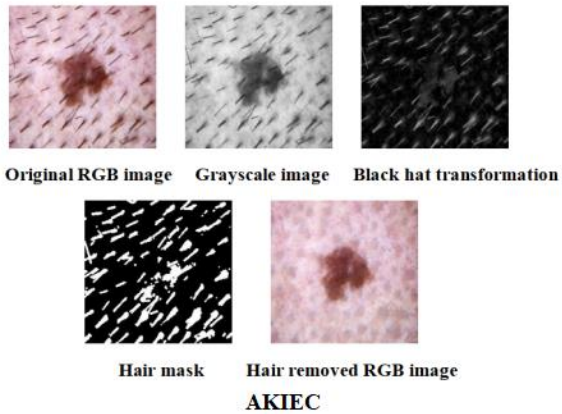


**Fig. 3:** Sample images for digital hair removal demonstrating artifact removal and enhanced lesion visibility for accurate analysis

Consider a set of dermoscopy images, where X demonstrates the image domain. All pixels $x_i$ within the domain, have a membership function assigned as $u_{ij}$, where j represents the class index. FCM aims to determine the $c_j$ cluster center that characterizes the distribution of pixels for a given set of images. The objective is to reduce the following objective function, which is expressed in Eq. (1):

$$J(U,C) = \sum_{i=1}^{N}\sum_{j=1}^{M} u_{ij}^{m}||x_i - c_j||^2 \quad (1)$$

Where J (U, C) indicates the objective function to be decreased, N represents the total number of pixels in the image, M denotes the number of classes, $u_{ij}$ determines the membership value of the class j in pixel $x_i$, and m denotes the fuzziness exponent. Beginning with the estimate of the initial cluster center, which is denoted as $c_j$, the membership values are calculated for each pixel, which represents the likelihood of belonging to all the classes. The cluster centers are recalculated using membership values, and it is checked whether the model has attained convergence; if not, the membership calculation is repeated, and the process is updated by the cluster center. Once convergence is attained, the model terminates, which provides the membership value $u_{ij}$ and cluster center $c_j$. Fig. 4 exhibits the mask and segmented images from the HAM10000 dataset, which are fed into the classification process.

### *Classification*

The segmentation images are fed as input to the PDNLCNN for classifying skin cancer, where the CNN extracts local lesion features and the PDNL captures angular and radial dependencies, leading to a more robust and accurate classification. CNN (Vega-Huerta et al., 2025) is chosen because it automatically extracts discriminative features such as the shape, texture, and color variations of lesions, which are significant for an accurate diagnosis. However, conventional CNNs capture only local features, which limits their applicability across lesions. Classical Non-Local (NL) operates in Cartesian coordinates (x, y) and captures long-range spatial dependencies uniformly over the feature map. However, NL does not process in radial symmetry and circular growth patterns, which affects model performance. DNL solves this by dividing attention into unary and pairwise components that enhance representation learning. But DNL still processes in Cartesian space and does not involve lesion-aware geometric modeling. The proposed PDNLCNN transforms feature maps into polar coordinates ($r$, $\theta$) to disentangle attention computation. To overcome this issue, a PDNL block is introduced, where the features are transformed into polar coordinates to capture angular and radial relationships effectively. This polar representation improves the ability of the network to explore lesion symmetry and structural patterns, which minimizes the irrelevant background information and provides richer contextual relationships. Overall, integrating PDNL with CNN enables both local feature learning and global structure, which results in more accurate and robust skin cancer classification. The detailed process of the proposed PDNLCNN for classifying skin cancer is described below, and its figure is shown in Fig. 5.

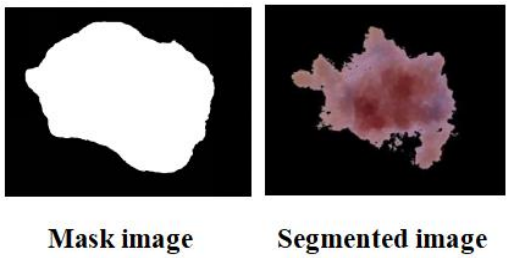


**Fig. 4:** Sample mask and segmented images generated from the HAM10000 dataset

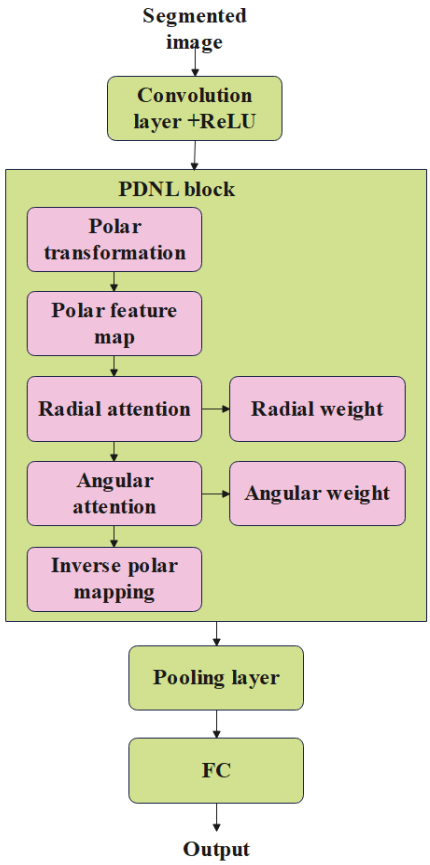


**Fig. 5:** Structure of the proposed PDNLCNN method to classify skin cancer

Convolution layer: This layer is used to extract the local features using Eq. (2), such as textures, patterns, and edges from the segmented images automatically. This creates a network to learn hierarchical representations that are crucial for accurate performance. This layer employs 5 convolutional layers (Conv1 to Conv5) with $3 \times 3$ kernels, strides of 1, and increasing filters from 32 to 512, which capture features from edges to global lesion patterns:

$$y_i = w_i \times x_i + b_i \; for \; i = 1, 2, \ldots, N \quad (2)$$

Where $y_i$ indicates the corresponding $i^{th}$ layer output, $x_i$ represents input for the $i^{th}$ layer, $w_i$ demonstrates the weight of the $i^{th}$ layer, $N$ determines the number of filters, and $b_i$ illustrates the $i^{th}$ bias.

Activation function: Rectified Linear Unit (ReLU) is used capture non-linear patterns that output 0 for all negative input values and return the same value for positive inputs, which is calculated using Eq. (3):

$$y = max(0, x) \quad (3)$$

Where y represents the ReLU output and x indicates the input.

PDNL: DNL block has the ability to model long-range dependencies more effectively, which allows the network to better capture global contextual information. Consider $X_m$ representing input features at the position $m$, and output features $Y_m$ of DNL are calculated using Eq. (4):

$$Y_m = \sum_{n \, \epsilon \, \Omega} M(X_m, X_n) g(X_n) \quad (4)$$

Where $M$ determines a set of pixels in the feature map of $\mathrm{H} \times \mathrm{W}$, and $g(.)$ indicates value transformation function with a parameter $W_v$, and $(X_m, X_n)$ represents an embedding similarity function from pixel $n$ (key pixel) to pixel $m$ (query pixel), as formulated in Eqs. (5) and (6):

$$M(X_m, X_n) = \sigma(q_m^T k_n) \quad (5)$$

$$\sigma(q_m^T k_n) = \sigma(u_q^T k_n + (q_m - u_q)^T (k_n - u_k)) \quad (6)$$

Where $q_m$ indicates the query pixel embedding $m$, $\sigma(.)$ determines the Softmax function, and the $k_n$ denotes the key embedding of the pixel $n$. In Equation (6), the initial term illustrates a unary relation, and the 2nd term demonstrates a pairwise relation between the key and query pixels. However, DNL operates in Cartesian coordinates, which is inappropriate for radial and circular patterns observed in skin lesions. Consequently, it is difficult to exploit the boundary structure and lesion symmetry fully. To solve this, PDNL is used, which transforms the features into polar coordinates and captures dependencies in both angular and radial directions. This polar representation aligns with the inherent process of skin lesions, which enhances the overall classification accuracy. Because skin lesions have circular and radial structures, the feature map is converted from Cartesian $(\mathrm{x}, \mathrm{y})$ to polar coordinates $(\mathrm{r}, \theta)$ around the lesion center $(\mathrm{x}_0, \mathrm{y}_0)$. The PDNLCNN integrates CNN and PDNL with a novel transformation of Cartesian into polar coordinates, designed to capture the unique characteristics of skin lesions. The mathematical formulas for $\mathrm{r}, \theta$ are expressed by Eqs. (7) and (8), respectively:

$$\mathrm{r} = \sqrt{(\mathrm{x} - \mathrm{x}_0)^2 + (\mathrm{y} - \mathrm{y}_0)^2} \quad (7)$$

$$\theta = \arctan\left(\frac{\mathrm{y} - \mathrm{y}_0}{\mathrm{x} - \mathrm{x}_0}\right) \quad (8)$$

This shows the polar feature tensor $X^{polar} \, \epsilon \, R^{C \times R \times T}$, where $R$ and $T$ represent the radial and angular samples, respectively. Linear embeddings are then used to acquire the keys $K = \mathrm{W_k} X^{polar}$, queries $\mathrm{Q} = \mathrm{W_q} X^{polar}$, and the values $V = \mathrm{W_v} X^{polar}$. In PDNL, the pairwise relation is factorized into radial and angular dependencies using Eqs. (9) and (10), respectively:

$$\mathrm{A_r}(\mathrm{r_m}, \mathrm{r_n}) = \mathrm{softmax}(\mathrm{Q_r}(\mathrm{r_m})^{\mathrm{T}} \mathrm{K_r}(\mathrm{r_n})) \quad (9)$$

$$\mathrm{A_\theta}(\theta_\mathrm{m}, \theta_\mathrm{n}) = \mathrm{softmax}(\mathrm{Q_\theta}(\theta_\mathrm{m})^{\mathrm{T}} \mathrm{K_\theta}(\theta_\mathrm{n})) \quad (10)$$

These attention maps capture the local and global dependencies along with the angle and radius, and the fused attention map is employed using Eq. (11):

$$\mathrm{A} = \mathrm{A_r} + \mathrm{A_\theta} + \mathrm{U} \quad (11)$$

Where U denotes unary attention, and contextualized features are aggregated using Eq. (12):

$$Y^{polar} = A.V \quad (12)$$

Finally, the projection and residual connections are computed using Eq. (13), and the features are mapped back to the Cartesian space and fed into the pooling process:

$$Z^{polar} = LN(X^{polar} + W_m Y^{polar}) \quad (13)$$

Pooling layer and Fully Connected (FC): This layer minimizes the spatial dimensions of feature maps by calculating the average value within each pooling region. This assists in minimizing the computational complexity while retaining the most significant global features. SoftMax is employed to produce a probability distribution function for classification. The classification layer assigns each feature to a class, depending on the probability distribution. The output size of the previous layer

evaluates the number of classes, and then FC produces the final class probabilities.

The hyperparameter values are chosen based on a grid search to ensure optimal performance. A learning rate of 0.001 with the Adam optimizer is chosen to balance rapid convergence and stable training, and a dropout of 0.4 is used to solve the overfitting issue. The ReLU activation function is employed to introduce non-linearity by avoiding vanishing gradient issues, and 100 epochs with a categorical cross-entropy loss function ensure effective learning for multi-class classification. Algorithm 1 presents a pseudocode of the proposed PDNLCNN to ensure reproducibility.

**Algorithm 1**

Input: Dermoscopic image datasets $D$ = {HAM10000, ISIC2019}
Output: Classified lesion type

Start
Step 1: Dataset
- i) Load dataset $D$
- ii) Split $D$ into the training and testing set

Step 2: Preprocessing

For each image $I$ in $D$ do
- i) Resize $I$ to 256×256 pixel
- ii) Utilize the morphological black-hat transformation.
- iii) Generate a hair mask from the transformation and perform in-painting.
- iv) Store the preprocessed image.

End For

Step 3: Segmentation using FCM

Initialize the number of clusters.
Initialize fuzziness coefficients
Randomly initialize cluster centers

while (not converged) do
- For each pixel in the preprocessed image, do
  - For each cluster, do
  - Compute membership value:
  - End For
- End For
- For each cluster, do
  - Update cluster center:
- End For

End while
Generate segmentation mask
Segmented image

Step 4: Classification using PDNLCNN

Initialize CNN layers (Conv, ReLU, Pooling)

For each segmented image, do
- i) Apply a convolutional layer and ReLU.
- ii) Utilize PDNL
  - a) Convert features from Cartesian to polar coordinates.
  - b) Calculate radial attention
  - c) Compute angular attention
  - d) Fuse attention maps
  - e) Aggregate contextualized features
  - f) Integrate features
- iii) Apply average pooling
- iv) Flatten pooled features
- v) Employ FC layers
- vi) Calculate class probabilities by utilizing SoftMax.

End For

Classify lesion type
End

## Results

The PDNLCNN is simulated by employing the MATLAB 2024b environment with an Intel i5 processor, 64 GB Random-Access Memory (RAM), and Windows 10 operating system. The experimental setup employs a batch size of 32 with libraries TensorFlow, Keras, NumPy, and Scikit-learn to ensure reproducibility. Accuracy, specificity, recall, F1-score, and precision are utilized for evaluating model performance with Eqs. (14) to (18). The ISIC2019 dataset is used for generalizability analysis to determine the unseen data:

$$\text{Accuracy}= \frac{TP+TN}{TP+TN+FP+FN}\times 100 \quad (14)$$

$$\text{Specificity}= \frac{TN}{TN+FP}\times 100 \quad (15)$$

$$\text{Recall}= \frac{TP}{TP+FN}\times 100 \quad (16)$$

$$\text{Precision}= \frac{TP}{TP+FP}\times 100 \quad (17)$$

$$\text{F1-Score}= \frac{2TP}{2TP+FP+FN}\times 100 \quad (18)$$

Where TP demonstrates True Positives, FP determines False Positives, FN determines False Negatives, and TN denotes True Negatives.

### *Performance Analysis*

Table 2 represents the performance evaluation of k-fold validation. K = 5 achieves superior accuracy owing to the balance between variance and bias in the K-Nearest Neighbor (KNN) model. When k = 3, the model becomes too sensitive to outliers and noise, which results in classification. Moreover, larger values such as k = 7 and 9, and over-smooth decision boundaries cause the model to lose significant local patterns. At k = 5, the model captures the appropriate neighborhood information that maintains the sensitivity to the local class structure. This optimal balance

enables better generalization and superior accuracy.

Table 3 represents the performance analysis of the computational complexity. The proposed PDNLCNN obtains the training times of 2.0063s and 2.0952s because polar transformation minimizes redundancy by concentrating on angular and radial representations. This enables the PDNL block to capture global dependencies more effectively and avoids the quadratic cost of non-local operations. By disentangling the attention into radial, unary, and angular terms, the model processes the features that require fewer computations. Furthermore, the integration of CNN with PDNL enables the learning of local features and minimizes unwanted computations by maintaining high classification performance.

Table 1 presents the performance evaluation of different classification techniques. Compared to existing techniques such as the autoencoder, Deep Neural Network (DNN), ResNet, CNN, channel attention ResNet, Vision Transformer (ViT), and swin transformer, the proposed PDNLCNN obtains high accuracy of 99.21% on the HAM10000 dataset and 98.65% on the ISIC2019 dataset, owing to the integration of the benefits of CNN in extracting the fine-grained local features with the global contextual ability of PDNL. By transforming features into polar coordinates, PDNL captures angular and radial dependencies effectively, which aligns with the symmetry and geometry of the skin lesions. This assists in preserving boundary information and minimizing the effects of inappropriate background information. Furthermore, the disentanglement of pairwise and unary terms ensures better representation of both pixel-to-pixel relationships and global information. Existing methods capture local features in Cartesian space, which does not align with the radial and circular structure of skin lesions. This results in loss of fine boundary information, redundant representation, and minimizes subtle discrimination and overlapping lesion patterns. Hence, PDNLCNN achieves better performance compared to existing methods.

**Table 1:** Performance analysis of different classification methods for skin cancer classification on HAM10000 and ISIC2019 datasets

| Dataset | Methods | Accuracy (%) | Recall (%) | Precision (%) | Specificity (%) | F1-score (%) |
|---|---|---|---|---|---|---|
| HAM10000 | Auto encoder | 92.45 | 92.15 | 92.13 | 92.45 | 92.47 |
| | DNN | 95.74 | 95.87 | 95.32 | 95.654 | 95.32 |
| | ResNet | 97.47 | 97.576 | 97.47 | 97.75 | 97.34 |
| | CNN | 98.46 | 98.76 | 98.21 | 98.14 | 98.52 |
| | Channel attention ResNet | 98.53 | 98.41 | 98.31 | 98.62 | 98.36 |
| | ViT | 98.85 | 98.80 | 98.72 | 98.90 | 98.76 |
| | Swin transformer | 98.45 | 98.38 | 98.15 | 98.55 | 98.44 |
| | NLCNN | 98.62 | 98.58 | 98.26 | 98.85 | 98.41 |
| | PDNLCNN | 99.21 | 99.05 | 99.63 | 99.14 | 99.25 |
| ISIC2019 | Auto encoder | 89.35 | 87.23 | 88.26 | 89.32 | 89.65 |
| | DNN | 92.65 | 92.67 | 93.65 | 92.64 | 92.54 |
| | ResNet | 95.76 | 95.45 | 95.86 | 95.43 | 95.87 |
| | CNN | 97.65 | 97.35 | 97.52 | 97.63 | 97.47 |
| | Channel attention ResNet | 98.10 | 97.95 | 98.12 | 98.25 | 98.03 |
| | ViT | 97.95 | 97.82 | 97.58 | 97.86 | 97.69 |
| | Swin transformer | 98.02 | 97.86 | 97.62 | 97.99 | 97.73 |
| | NLCNN | 97.08 | 97.90 | 97.85 | 97.74 | 97.87 |
| | PDNLCNN | 98.65 | 98.22 | 98.54 | 98.95 | 98.85 |

**Table 2:** Evaluation of k-fold cross-validation on HAM10000 and ISIC2019 datasets for classification performance

| Dataset | K-fold | Accuracy (%) | Recall (%) | Precision (%) | Specificity (%) | F1-score (%) |
|---|---|---|---|---|---|---|
| | k= 3 | 96.21 | 96.32 | 96.52 | 96.76 | 96.32 |
| | k=5 | 99.21 | 99.05 | 99.63 | 99.14 | 99.25 |
| | k=7 | 98.35 | 98.43 | 98.12 | 98.32 | 98.42 |
| HAM10000 | k=9 | 97.65 | 97.35 | 97.32 | 97.32 | 97.21 |
| | k= 3 | 95.367 | 95.325 | 95.784 | 95.5539 | 95.487 |
| | k=5 | 98.65 | 98.22 | 98.54 | 98.95 | 98.85 |
| | k=7 | 97.264 | 96.236 | 97.258 | 96.7443 | 97.365 |
| ISIC2019 | k=9 | 96.349 | 95.436 | 96.065 | 95.7495 | 96.461 |

**Table 3:** Evaluation of computational complexity in terms of run time, memory consumption, training time, and inference time on different datasets

| Dataset | Methods | Run time (s) | Memory consumption (MB) | Training time (s) | Instance time (s) |
|---|---|---|---|---|---|
| HAM10000 | Auto encoder | 12.1378 | 33.85 | 2.4378 | 12.0680 |
| | DNN | 1.6193 | 12.45 | 9.4365 | 0.0146 |
| | ResNet | 1.7173 | 5.48 | 3.5465 | 0.0052 |
| | CNN | 2.5768 | 8.54 | 3.6574 | 0.0075 |
| | Channel attention ResNet | 4.1250 | 7.20 | 4.1250 | 0.0068 |
| | ViT | 5.8420 | 18.45 | 12.5500 | 0.0125 |
| | Swin transformer | 4.9500 | 14.30 | 9.8800 | 0.0095 |
| | NLCNN | 4.0563 | 5.26 | 5.6398 | 0.0059 |
| | PDNLCNN | 3.7376 | 5.53 | 2.0063 | 0.0035 |
| ISIC2019 | Auto encoder | 11.9927 | 0.02 | 21.4812 | 0.0092 |
| | DNN | 2.5187 | 5.50 | 8.7834 | 0.0057 |
| | ResNet | 2.4839 | 5.49 | 2.5439 | 0.0172 |
| | CNN | 1.3454 | 6.44 | 2.31345 | 0.0104 |
| | Channel attention ResNet | 2.1500 | 11.80 | 3.4500 | 0.0088 |
| | ViT | 4.2200 | 16.20 | 10.1500 | 0.0155 |
| | Swin transformer | 3.8500 | 12.10 | 8.4400 | 0.0110 |
| | NLCNN | 1.5896 | 10.25 | 3.2568 | 0.0080 |
| | PDNLCNN | 0.7388 | 9.52 | 2.0952 | 0.0045 |

Table 4 demonstrates performance analysis of different segmentation methods on HAM10000 and ISIC2019 datasets. Compared to other methods, FCM obtains a high Dice score due to assigning soft membership values to pixels that enable partial belonging to the background and lesion. This accurately captures fuzzy, low-contrast boundaries, minimizes misclassification, and obtains a high dice score.

Table 5 demonstrates cross-dataset validation training on ISIC-2019 and testing on the HAM10000 dataset to evaluate the generalization ability. ISIC2019 is chosen for training due to containing a high number of images, whereas HAM10000 is employed for testing because it involves a smaller number of images. Compared to existing methods, the proposed method obtains better performance on unseen data. This represents its superior ability to generalize and capture appropriate lesion features effectively.

Table 6 shows the ablation study analysis to isolate the impact of each component in the proposed method. Compared to other variants, the proposed method achieves better performance by capturing fine-grained local and global angular radial lesion dependencies. This polar transformation provides symmetric and circular structures of skin lesions that preserve boundary information and enhance classification performance.

Figure 6 displays the performance evaluation of the confusion matrix for PDNLCNN. In both cases, most of the samples are classified correctly, with certain misclassifications occurring in visually similar classes such as Melanoma (MEL) and Benign Keratosis (BKL). The performance of ISIC2019 indicates robustness across a wide range of lesion types, which maintains a robust performance and obtains reliable skin cancer classification.

**Table 4:** Performance analysis of different segmentation methods on HAM10000 and ISIC2019 datasets

| Methods | Dice score (%) | IoU (%) | Pixel Accuracy (%) | Boundary F1 (%) |
|---|---|---|---|---|
| | | HAM10000 | | |
| Otsu | 76.8 | 64.1 | 90.5 | 68.9 |
| Region Growing | 78.9 | 66.5 | 92.5 | 70.2 |
| K-means | 81.5 | 70.2 | 92.1 | 74.8 |
| U-Net | 84.8 | 74.2 | 93.1 | 78.5 |
| FCM | 87.2 | 78.5 | 94.6 | 82.3 |
| | | ISIC2019 | | |
| Otsu | 74.2 | 61.3 | 89.7 | 66.5 |
| Region Growing | 76.3 | 63.8 | 91.4 | 72.9 |
| K-means | 79.3 | 68.5 | 91.4 | 72.9 |
| U-Net | 82.9 | 71.5 | 91.8 | 76.4 |
| FCM | 85.7 | 76.1 | 93.2 | 80.1 |

**Table 5:** Analysis of cross-dataset validation training on ISIC2019 and testing on HAM10000 datasets to evaluate generalization on unseen data

| Method | Accuracy (%) | F1-Score (%) | Precision (%) | Recall (%) | Specificity (%) |
|---|---|---|---|---|---|
| ResNet | 89.45 | 88.12 | 89.05 | 88.54 | 89.92 |
| CNN | 91.23 | 90.45 | 91.02 | 90.88 | 91.56 |
| DCNN | 92.67 | 91.88 | 92.15 | 91.92 | 93.10 |
| Channel Attention ResNet | 93.42 | 92.75 | 93.10 | 92.88 | 94.05 |
| ViT | 94.15 | 93.60 | 93.85 | 93.42 | 94.88 |
| Swin | 95.20 | 94.38 | 94.75 | 94.10 | 95.92 |
| NLCNN | 95.24 | 94.48 | 94.85 | 94.12 | 95.99 |
| PDNLCNN | 95.84 | 94.92 | 95.12 | 94.85 | 96.48 |

**Table 6:** Ablation study analysis isolating the contribution of each component for the proposed method

| Method | Datasets | Accuracy (%) | F1-Score (%) | Precision (%) | Recall (%) | Specificity (%) |
|---|---|---|---|---|---|---|
| CNN | HAM10000 | 98.46 | 98.52 | 98.21 | 98.76 | 98.14 |
| NL-CNN | | 98.62 | 98.41 | 98.26 | 98.58 | 98.85 |
| DNL-CNN | | 98.45 | 98.12 | 98.33 | 98.01 | 98.99 |
| FCM+PDNL+CNN | | 99.21 | 99.25 | 99.63 | 99.05 | 99.14 |
| CNN | ISIC2019 | 97.65 | 97.47 | 97.52 | 97.35 | 97.63 |
| NL-CNN | | 97.08 | 97.87 | 97.85 | 97.90 | 97.87 |
| DNL-CNN | | 97.58 | 97.96 | 97.96 | 97.95 | 97.98 |
| FCM+PDNL+CNN | | 98.65 | 98.85 | 98.54 | 98.22 | 98.95 |

Fig. 7 depicts the analysis of the Receiver Operating Characteristics (ROC) curve for the proposed method. All classes obtain Area Under Curve (AUC) values between 0.99 and 1.00, which shows that the model correctly identifies negative and positive cases with high accuracy. These results indicate that the proposed PDNLCNN obtains reliable and accurate skin cancer classifications for both datasets.

Fig. 8 demonstrates the performance evaluation of the statistical analysis test. The t-test is a statistical method used to determine significant differences between the means of two groups. The p-value obtained from the t-test is small, indicating a difference in performance between the two models. Calculating the p-value assists in establishing whether the proposed method is statistically significant rather than random variations, which enables the model's enhancement to be reliable and valid.

Fig. 9 illustrates the standard deviation analysis for the proposed PDNLCNN. Standard deviation is a statistical measure to evaluate the amount of variation in a dataset. Model analysis reflects the consistency of performance measures, namely precision, F1-score, accuracy, recall, and specificity across multiple runs. A lower standard deviation indicates that the proposed model is stable and reliable, whereas a higher value indicates greater variability. The PDNLCNN not only achieves better accuracy but also maintains consistent outcomes over different datasets.

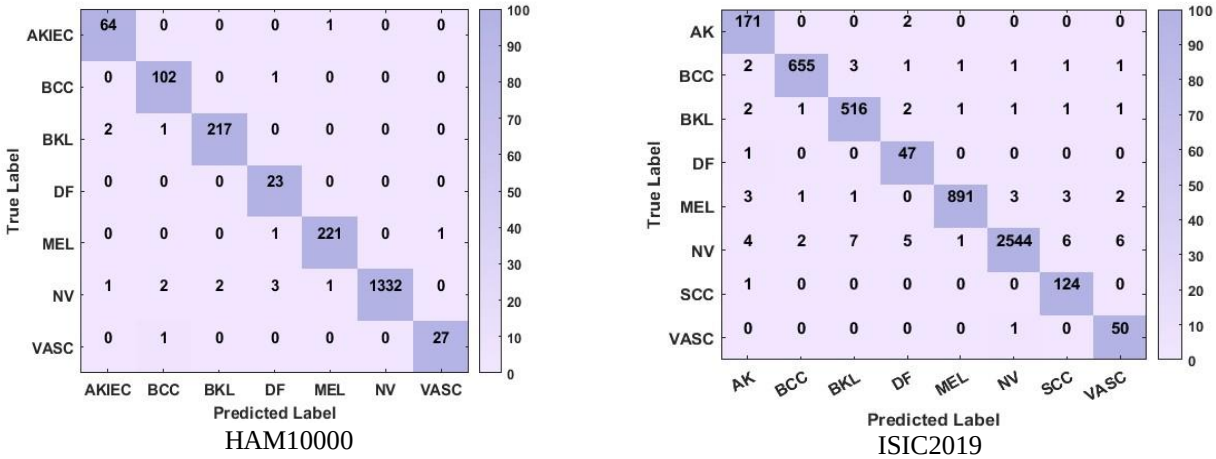


**Fig. 6:** Analysis of the confusion matrix for the proposed method, which shows classification performance

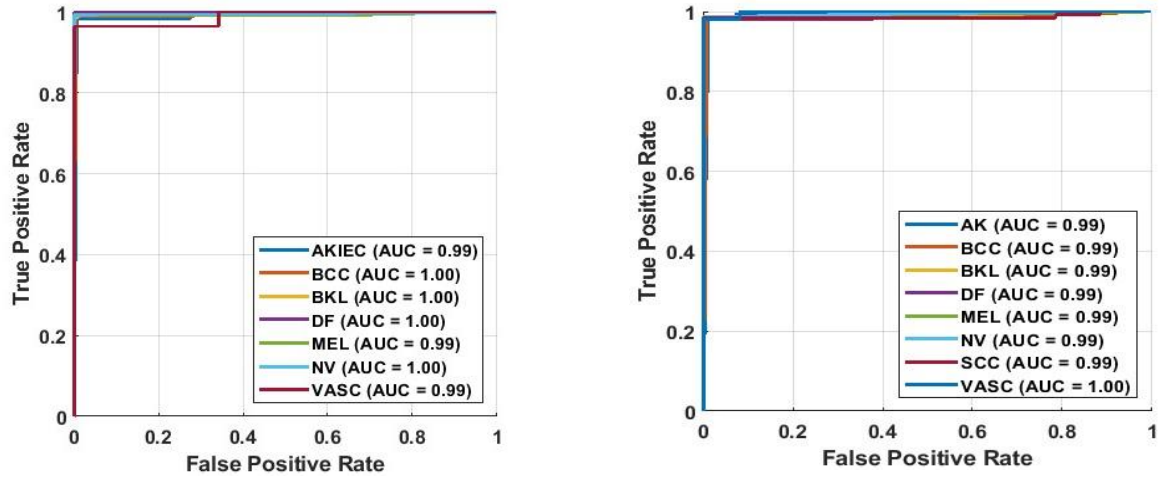


HAM10000 ISIC2019

**Fig. 7:** Performance analysis of the ROC curve, which illustrates classification performance

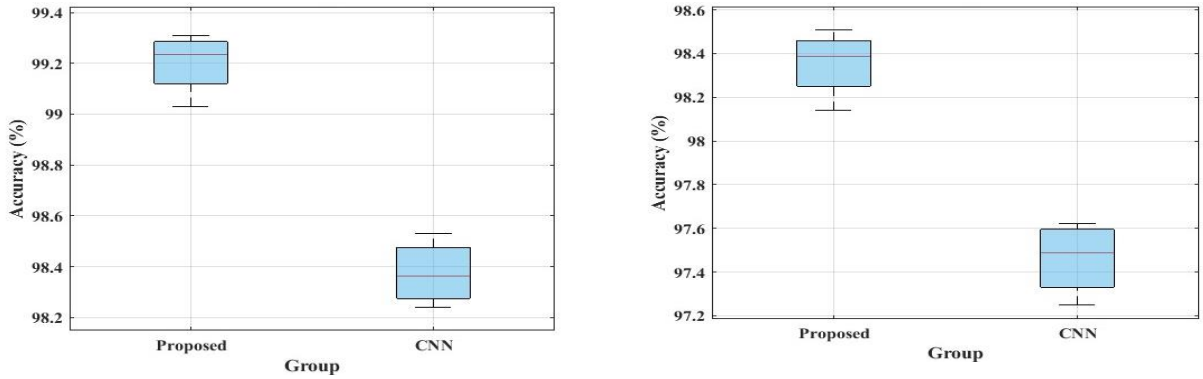


HAM10000 ISIC2019

**Fig. 8:** Evaluation of p-value from t-test for the proposed method

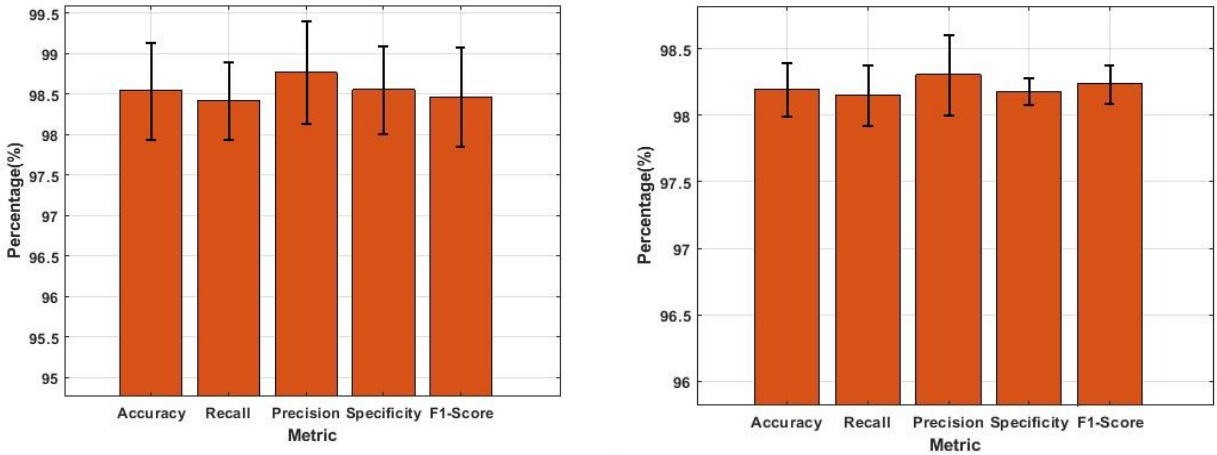


HAM10000 ISIC2019

**Fig. 9:** Analysis of standard deviation for the proposed PDNLCNN on different datasets

### *Comparative Analysis*

Table 7 illustrates a comparative evaluation of existing techniques utilizing the HAM10000. Compared with existing methods, such as (Kumar et al., 2024b; Ibrahim et al., 2025; Houssein et al., 2024; Al Mahmud et al., 2024; Kumar et al., 2024a; Abohashish et al., 2025), the proposed PDNLCNN obtains better accuracy of 99.21% on HAM10000 because it integrates CNN to extract local lesion features with PDNL's strength to capture global radial and angular dependencies. This polar-aware process enhances the boundary preservation and structural patterns, resulting in more discriminative feature learning. Hence, the proposed method obtains better accuracy, reliability, and robustness compared to the existing methods. The specificity of the proposed method is slightly lower due to certain benign samples with features similar to malignant lesions being misclassified. GLCM+LBP+GWO achieves high accuracy due to handcrafted features and optimized feature selection, strongly suitable for dominant classes, which leads to marginally better accuracy. However, existing methods fail to achieve high recall, precision, and F1-score due to manual features, and shallow representation does not capture subtle information, overlapping, and fine-grained lesion patterns. Hence, while accuracy is high, the imbalance between FP and FN minimizes performance in other performance metrics. The proposed method obtains better performance in recall, precision, and F1-score due to capturing long-range dependencies and fine-grained lesion variations. This representation enhances discrimination among similar classes, minimizes misclassification, and maintains reliable and balanced results.

**Table 7:** Comparative evaluation of existing methods with the proposed method using the HAM10000 dataset

| Methods | Accuracy (%) | Recall (%) | Precision (%) | Specificity (%) | F1-score (%) |
|---|---|---|---|---|---|
| GLCM+LBP+GWO (Kumar et al., 2024b) | 99.54 | 98.79 | 99.44 | N/A | 99.11 |
| Ensemble model with TTA (Ibrahim et al., 2025) | 94.49 | 94.49 | 95.07 | N/A | 94.68 |
| DCNN (Houssein et al., 2024) | 98.5 | 98.51 | 98.56 | 99.73 | 98.48 |
| SkinNet-14 (Al Mahmud et al., 2024) | 97.85 | N/A | N/A | N/A | 97.92 |
| Optimized hybrid MobileNet-V3 (Kumar et al., 2024a) | 98.86 | 95.27 | 97.84 | N/A | 97.32 |
| CNN-LSTM-based patch-wise (Abohashish et al., 2025) | 97 | 94.76 | 92.23 | N/A | 94.47 |
| Proposed PDNLCNN | 99.21 | 99.05 | 99.63 | 99.14 | 99.25 |

### *Discussion*

A strength of PDNLCNN and the limitations of existing methods are explained in this subsection. A limitation of existing techniques, such as GLCM+LBP+GWO (Kumar et al. 2024b), is that they are based on manually engineered features that fail to capture deep hierarchical patterns in intricate lesion images. The ensemble (Ibrahim et al., 2025) suffers from a high computational cost and memory usage owing to multiple deep networks with millions of parameters. DCNN (Houssein et al., 2024) struggles with overfitting while being trained on the limited skin cancer data. SkinNet-14 (Al Mahmud et al., 2024) is limited by its relatively shallow architecture, which limits its ability to learn intricate hierarchical features. U-Net (Kumar et al., 2024a) is limited by the reliance on pixel-level annotations, which makes it sensitive to boundary irregularities in skin lesions. The proposed PDNLCNN overcomes the limitations of the existing methods by integrating local and global feature learning effectively. The CNN captures fine-grained local information, whereas the PDNL operates in polar coordinates that align with the circular and radial structures of skin lesions. This enables the model to better preserve boundary information and capture symmetry patterns that are significant to differentiate malignant lesions from benign lesions. Moreover, PDNL minimizes the impact of inappropriate background pixels, thereby making the model more robust. Overall, these strengths ensure that PDNLCNN provides accurate and reliable skin cancer classification.

The proposed PDNLCNN represents significant benefits in terms of accuracy, efficiency, and robustness. The proposed method obtains high accuracy through effectively focusing on appropriate lesion features by minimizing irrelevant background pixels. A polar coordinate transformation minimizes redundancy by angular and radial representation that enhances feature effectiveness. Moreover, disentangling the representation into unary, radial, and angular components enables the

model to capture global dependencies without quadratic cost related to the classical NL block. As a result, PDNLCNN obtains a training time of 2.0063 s on the HAM10000 dataset compared to existing methods, which demonstrates computational efficiency.

## Conclusion

This research proposed a PDNLCNN for categorizing skin cancer accurately. PDNLCNN enhanced the ability of the model to capture spatial dependencies, which minimized redundancy in the feature representation. It disentangled the appropriate polar information that enabled the network to concentrate on subtle lesion patterns and boundary irregularities that were significant for an accurate diagnosis. This enhanced the feature discrimination and resulted in superior classification accuracy and robustness against variations in the appearance of the skin lesions. Moreover, the preprocessing technique, resizing, ensured uniform input dimensions that increased the computational effectiveness, whereas digital hair removal eliminated the occlusions caused by hair, which provided a clearer visibility of the lesion structure. By performing this process, the proposed PDNLCNN obtained a superior accuracy of 99.21% on the HAM10000 dataset when compared to the existing methods, such as DCNN. Since this research focuses on benchmarking datasets to evaluate the proposed method, real-world applicability will be considered as future work with cross-device validation between clinical scanners and mobile dermoscopy.

## Acknowledgment

The authors sincerely thank Bharath Institute of Higher Education and Research, Chennai, and Bharath Institute of Science and Technology, Chennai, for providing the necessary facilities and support to carry out this research. The authors are also grateful to their colleagues and peers for their valuable feedback and encouragement during the preparation of this work.

## Funding Information

This research did not receive any specific grant from funding agencies in the public, commercial, or not-for-profit sectors.

## Author's Contributions

**Usha Thirugnanam:** Conceptualization, methodology, data collection, and drafting of the manuscript.

**Nalini Joseph:** Data analysis, literature review, editing, and finalization of the manuscript.

Both authors read and approved the final version of the manuscript.

## Ethics

This article does not involve any studies with human participants or animals performed by any of the authors. The authors affirm that the work is original, has not been published previously, and is not under consideration elsewhere.

## References

Abdulkadhim, A. A. A., Abbas, F. N., & Shawi, R. T. (2025). Deep Learning-based Hybrid ResNet50 and AlexNet Model for Skin Cancer Classification. *International Journal of Intelligent Engineering and Systems*, *18*(6), 892–903. https://doi.org/10.22266/ijies2025.0731.55

Abdulredah, A. A., Fadhel, M. A., Alzubaidi, L., Duan, Y., Kherallah, M., & Charfi, F. (2025). Towards unbiased skin cancer classification using deep feature fusion. *BMC Medical Informatics and Decision Making*, *25*(1), 48. https://doi.org/10.1186/s12911-025-02889-w

Abohashish, S. M. M., Amin, H. H., & Elsedimy, E. I. (2025). Enhanced melanoma and non-melanoma skin cancer classification using a hybrid LSTM-CNN model. *Scientific Reports*, *15*(1), 24994. https://doi.org/10.1038/s41598-025-08954-8

Aboulmira, A., Hrimech, H., Lachgar, M., Hanine, M., Garcia, C. O., Mezquita, G. M., & Ashraf, I. (2025). Hybrid Model with Wavelet Decomposition and EfficientNet for Accurate Skin Cancer Classification. *Journal of Cancer*, *16*(2), 506–520. https://doi.org/10.7150/jca.101574

Al Mahmud, A., Azam, S., Khan, I. U., Montaha, S., Karim, A., Haque, A., Zahid Hasan, M., Brady, M., Biswas, R., & Jonkman, M. (2024). SkinNet-14: a deep learning framework for accurate skin cancer classification using low-resolution dermoscopy images with optimized training time. *Neural Computing and Applications*, *36*(30), 18935–18959. https://doi.org/10.1007/s00521-024-10225-y

Alotaibi, A., & AlSaeed, D. (2025). Skin Cancer Detection Using Transfer Learning and Deep Attention Mechanisms. *Diagnostics*, *15*(1), 99. https://doi.org/10.3390/diagnostics15010099

Alqhtani, S. M., Soomro, T. A., Ali Shah, A., Aziz Memon, A., Irfan, M., Rahman, S., Jalalah, M., Almawgani, A. H. M., & Bade Eljak, L. A. (2024). Improved Brain Tumor Segmentation and Classification in Brain MRI with FCM-SVM: A Diagnostic Approach. *IEEE Access*, *12*, 61312–61335. https://doi.org/10.1109/access.2024.3394541

Attallah, O. (2024). Skin cancer classification leveraging multi-directional compact convolutional neural network ensembles and gabor wavelets. *Scientific Reports*, *14*(1), 20637. https://doi.org/10.1038/s41598-024-69954-8

Eliwa, E. H. I. (2025). Enhancing Skin Cancer Diagnosis Through Fine-Tuning of Pretrained Models: A Two-Phase Transfer Learning Approach. *International Journal of Breast Cancer*, *2025*(1), 4362941. https://doi.org/10.1155/ijbc/4362941

Faizi, M. I., & Adnan, S. M. (2024). Improved Segmentation Model for Melanoma Lesion Detection Using Normalized Cross-Correlation-Based *k*-Means Clustering. *IEEE Access*, *12*, 20753–20766. https://doi.org/10.1109/access.2024.3360223

Gajbhiye, N. N., Kadu, S. R., & Sadruddin, S. (2025). An Efficient Skin Cancer Detection and Classification Using DenseNet-121 with Attention Mechanism. *International Journal of Intelligent Engineering and Systems*, *18*(5), 745–759. https://doi.org/10.22266/ijies2025.0630.52

HAM10000. (2025). Dataset: *Kaggle*.

Himel, G. M. S., Islam, Md. M., Al-Aff, Kh. A., Karim, S. I., & Sikder, Md. K. U. (2024). Skin Cancer Segmentation and Classification Using Vision Transformer for Automatic Analysis in Dermatoscopy-Based Noninvasive Digital System. *International Journal of Biomedical Imaging*, *2024*(1), 3022192. https://doi.org/10.1155/2024/3022192

Houssein, E. H., Abdelkareem, D. A., Hu, G., Hameed, M. A., Ibrahim, I. A., & Younan, M. (2024). An effective multiclass skin cancer classification approach based on deep convolutional neural network. *Cluster Computing*, *27*(9), 12799–12819. https://doi.org/10.1007/s10586-024-04540-1

Ibrahim, A. T., Abdullahi, M., Kana, A. F. D., Mohammed, M. T., & Hassan, I. H. (2025). Categorical classification of skin cancer using a weighted ensemble of transfer learning with test time augmentation. *Data Science and Management*, *8*(2), 174–184. https://doi.org/10.1016/j.dsm.2024.10.002

Jaber, N. J. F., & Akbas, A. (2024). Melanoma skin cancer detection based on deep learning methods and binary Harris Hawk optimization. *Multimedia Tools and Applications*, *84*(22), 25709–25722. https://doi.org/10.1007/s11042-024-19864-8

khan, M. A., Ali, M. D., Mazhar, T., Shahzad, T., Rehman, W. U., Shahid, M., & Hamam, H. (2025a). An Advanced Deep Learning Framework for Skin Cancer Classification. *The Review of Socionetwork Strategies*, *19*(1), 111–130. https://doi.org/10.1007/s12626-025-00181-x

Khan, M. A., Rastogi, D., Johri, P., Al-Taani, A., Baghela, V. S., & Kumud. (2025b). Hybrid deep CNN model for multi-class classification of skin lesion. *Neural Computing and Applications*, *37*(23), 19479–19499. https://doi.org/10.1007/s00521-025-11409-w

Kumar, U. L., Simaiya, S., Sharma, Y. K., Kaswan, K. S., Brahma Rao, K. B. V., Maheswara Rao, V. V. R., Baliyan, A., Bijalwan, A., & Alroobaea, R. (2024a). A precise model for skin cancer diagnosis using hybrid U-Net and improved MobileNet-V3 with hyperparameters optimization. *Scientific Reports*, *14*(1), 1–23. https://doi.org/10.1038/s41598-024-54212-8

Kumar, H., Dwivedi, A., Mishra, A. K., Shukla, A. K., Sharma, B. K., Agarwal, R., & Kumar, S. (2024b). Transformer-based decoder of melanoma classification using hand-crafted texture feature fusion and Gray Wolf Optimization algorithm. *MethodsX*, *13*, 102839. https://doi.org/10.1016/j.mex.2024.102839

Mridha, K., Uddin, Md. M., Shin, J., Khadka, S., & Mridha, M. F. (2023). An Interpretable Skin Cancer Classification Using Optimized Convolutional Neural Network for a Smart Healthcare System. *IEEE Access*, *11*, 41003–41018. https://doi.org/10.1109/access.2023.3269694

Musthafa, M. M., T R, M., V, V. K., & Guluwadi, S. (2024). Enhanced skin cancer diagnosis using optimized CNN architecture and checkpoints for automated dermatological lesion classification. *BMC Medical Imaging*, *24*(1), 201. https://doi.org/10.1186/s12880-024-01356-8

Ozdemir, B., & Pacal, I. (2025). A robust deep learning framework for multiclass skin cancer classification. *Scientific Reports*, *15*(1), 4938. https://doi.org/10.1038/s41598-025-89230-7

Pandey, A., Teja, M. S., Sahare, P., Kamble, V., Parate, M., & Hashmi, M. F. (2024). Skin cancer classification using non-local means denoising and sparse dictionary learning based CNN. *Journal of Electrical Systems and Information Technology*, *11*(1), 36. https://doi.org/10.1186/s43067-024-00162-0

ISIC-2019. (2025). Dataset. *Kaggle*.

Raghavendra, P. V. S. P., Charitha, C., Begum, K. G., & Prasath, V. B. S. (2023). Deep Learning–Based Skin Lesion Multi-class Classification with Global Average Pooling Improvement. *Journal of Digital Imaging*, *36*(5), 2227–2248. https://doi.org/10.1007/s10278-023-00862-5

Saha, S., Hemal, M. M., Eidmum, M. Z. A., & Mridha, M. F. (2025). Knowledge distillation approach for skin cancer classification on lightweight deep learning model. *Healthcare Technology Letters*, *12*(1), e12120. https://doi.org/10.1049/htl2.12120

Toprak, A. N., & Aruk, I. (2024). A Hybrid Convolutional Neural Network Model for the Classification of Multi-Class Skin Cancer. *International Journal of Imaging Systems and Technology*, *34*(5), e23180. https://doi.org/10.1002/ima.23180

Vega-Huerta, H., Rivera-Obregón, M., Maquen-Niño, G. L. E., De-la-Cruz-VdV, P., Lázaro-Guillermo, J. C., Pantoja-Collantes, J., & Cámara-Figueroa, A. (2025). Classification Model of Skin Cancer Using Convolutional Neural Network. *Ingénierie Des Systèmes d Information*, *30*(02), 387–394. https://doi.org/10.18280/isi.300210

Yang, G., Luo, S., & Greer, P. (2023). A Novel Vision Transformer Model for Skin Cancer Classification. *Neural Processing Letters*, *55*(7), 9335–9351. https://doi.org/10.1007/s11063-023-11204-5